# Rotational motion in the molecular crystals meta- and ortho-carborane studied by deuteron nuclear magnetic resonance

**ARTICLE** *in* THE JOURNAL OF CHEMICAL PHYSICS · OCTOBER 2005

Impact Factor: 2.95 · DOI: 10.1063/1.2013254 · Source: PubMed



**4 AUTHORS**, INCLUDING:

Herbert Zimmermann
Max Planck Institute for Medical Research
**305** PUBLICATIONS **5,505** CITATIONS

SEE PROFILE

# Rotational motion in the molecular crystals *meta*- and *ortho*-carborane studied by deuteron nuclear magnetic resonance

Manfred Winterlich and Roland Böhmer
*Experimentelle Physik III and Interdisziplinäres Zentrum für Magnetische Resonanz, Universität Dortmund, 44221 Dortmund, Germany*

Gregor Diezemann
*Institut für Physikalische Chemie, Universität Mainz, 55099 Mainz, Germany*

Herbert Zimmermann
*Max Planck-Institut für Medizinische Forschung, 69120 Heidelberg, Germany*

(Received 27 April 2005; accepted 12 July 2005; published online 7 September 2005)

Spin-lattice and spin-spin-relaxation times, one- and two-dimensional spectra as well as two- and four-time correlation functions were measured for the molecular crystals *ortho*- and *meta*-carborane using deuteron nuclear magnetic resonance. It is found that in their noncubic phases these crystals exhibit highly anisotropic motions. In order to allow for a quantitative description of the motional geometry of the carboranes several stochastic models are formulated. By comparison of the model calculations with the experimental results it is found that the dynamics of these quasi-icosahedrally shaped molecules is governed by a composite reorientation process. Here the molecules perform threefold jumps around a molecule-fixed axis which itself can be tilted in four different directions with respect to a crystal-fixed axis. The tilt angle increases significantly with increasing temperature. On the basis of measurements of four-time stimulated-echo functions, implications for dynamic heterogeneity also in comparison with that of supercooled liquids are discussed. © *2005 American Institute of Physics*. [DOI: 10.1063/1.2013254]

## I. INTRODUCTION

The physics of glass-forming materials continues to be an area that attracts a lot of attention.[1,2] Part of the fascination of this subject stems from the fact that glassy behavior and often enough universal patterns show up in many branches of condensed-matter physics. This is because virtually each disordered state, when quenched fast enough, can be transferred into a glassy one. That is, one can cool down organic, semiconducting, metallic, etc., melts, and thus obtains structural glasses devoid of long-range translational order. However, when dealing with asymmetric constituents, glassy behavior can also arise if a well-defined center-of-mass lattice is present. This is the field of plastic or orientationally disordered crystals. When avoiding orientational ordering these can freeze into glassy crystals.[3,4] Furthermore, these latter systems bear a number of similarities with orientational glasses and spin glasses[5–8] for which, however, the ground state usually is highly degenerate. Spin and orientational glasses typically are crystals which are doped with interacting asymmetrical entities such as magnetic and electric dipole moments. Among the orientational glasses probably the mixed cyanides are those which were studied most extensively.[5] It should be noted that also systems without doping, e.g., pure cyanides, can exhibit glassy crystal phases.[9,10] Due to the restrictions imposed by the lattice symmetry the molecules constituting supercooled plastic crystals can only take on a finite set of orientations. This often facilitates the interpretation of the experimental results and the theoretical models formulated for their description.

Well-known examples of supercooled plastic crystals, that were recently studied by NMR methods, include cyanoadamantane[11,12] and the carboranes, namely, *ortho*-carborane (OCA) and *meta*-carborane (MCA). These carboranes form the subject of the present article. Apart from NMR (Refs. 13–17) the carboranes were studied by a number of methods such as calorimetry,[18,19] Raman scattering,[20] molecular-dynamics simulations,[21] by x-ray diffraction,[13] and last but not least by broadband dielectric investigations.[22–24] The sequence of phase transitions exhibited by the carboranes is summarized in Fig. 1. OCA and MCA melt at 570 and 546 K, respectively. Below this temperature they are stable in a face-centered-cubic phase (I). While upon cooling MCA directly transforms into an orthorhombic structure (at $T \approx 285$ K), for OCA a tetragonal phase (II), stable between 295 and 275 K, precedes the formation of the orthorhombic modification. For temperatures below 165 K, it has been reported[13] that the crystal symmetry of MCA is further reduced and that a monoclinic phase (III) becomes stable. For OCA the orthorhombic phase (III) transforms at 167 K, however, the symmetry of the low-temperature phase is obviously unknown.[13] It has been found that the transitions near 165 K can exhibit enormous hystereses.[16] For OCA the tetragonal phase was reported to form already above about 217 K upon reheating[13] which is quite different from the transition temperature observed upon cooling.

In previous publications we focused on the dynamics of MCA near its phase transitions[16] and on some aspects of dynamic heterogeneity of OCA (Refs. 17 and 25) which re-

 

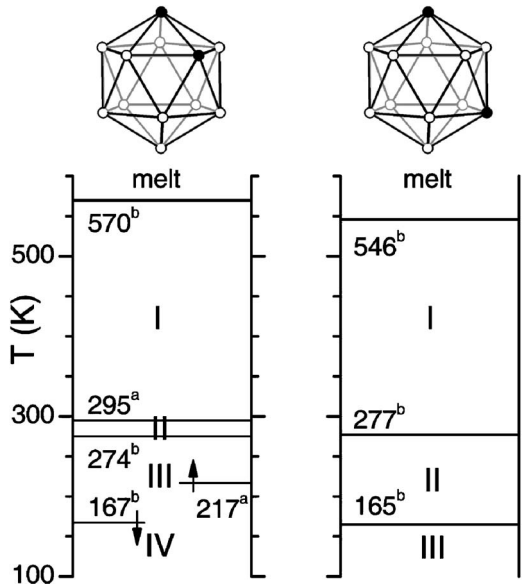


FIG. 1. Phase sequence of OCA (left-hand side) and MCA (right-hand side) under ambient pressure conditions. Sketches of the molecular structures are also included. The open vertices represent the boron atoms decorated by a proton and the closed vertices represent the carbon atoms which for the present study were labeled by deuterons. The phases are numbered with roman numerals. The transition temperatures, corresponding to the fully protonated species, are those given by Reynhardt and Froneman (Ref. 13) (marked by the letter a) and by Leites (Ref. 27) (marked by the letter b).

quire a detailed understanding of the motional geometry in these crystals. One of the goals of the present article is to provide additional experimental NMR data on these substances and, on this basis, to formulate suitable theoretical models to describe the molecular dynamics in the carboranes in some detail.

This paper is organized as follows: After noting a few experimental details, in Sec. III we present the experimental results. These include measurements of spin-lattice and spin-spin-relaxation times, one- and two-dimensional spectra, and finally two- and four-time correlation functions. Based on the wealth of experimental data, in Sec. IV we consider several stochastic models for their analysis. In Sec. V we then present the application of one of them, the tilt-jump model, which provides a consistent description of our data. Moreover, we discuss some implications also with respect to the related investigations on supercooled liquids. Finally in Sec. VI we summarize the results of the present study.

## II. EXPERIMENTAL DETAILS

The carborane specimens used for this study were selectively deuterated at those proton sites which are directly bonded to the carbon atoms. The procedure employed to deuterate MCA was described previously.[16] A similar route was used to label the ortho species, however, with protonated OCA as the starting material. The NMR investigations were carried out at a Larmor frequency of $\omega_L = 2\pi \times 40.2$ MHz using a home-built spectrometer and the length of the $\pi$ pulses typically was 5 $\mu$s.

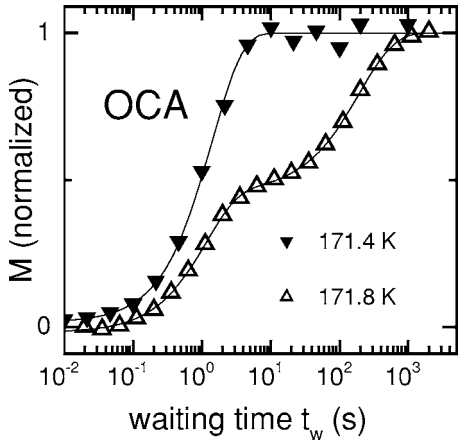


FIG. 2. Relaxation of the longitudinal magnetization $M(t_w)$ of OCA measured subsequent to saturation near $T = 172$ K. The data were recorded after cooling (closed symbols) and heating (open symbols) as described in the text. In both cases the measurements were carried out to very long waiting times $t_w$. The long time magnetizations were used to normalize the data.

## III. EXPERIMENTAL RESULTS

### A. Spin relaxation

In order to characterize the overall relaxation dynamics of OCA, we first measured the deuteron spin-lattice-relaxation times employing the saturation recovery technique and the spin-spin-relaxation times using a solid-echo sequence. A typical experimental result for the magnetization recovery $M(t)$ obtained after cooling from room temperature is shown in Fig. 2. It is seen that $M(t)$ is close to exponential. Similar data were obtained in a large temperature range and the resulting spin-lattice-relaxation times are presented in Fig. 3(a). At $T \approx 270$ K the tetragonal $\leftrightarrow$ orthorhombic phase transition leads to a discontinuity in $T_1$. In Fig. 3(b) we also present the spin-spin-relaxation times. Here a potential discontinuity may be partly masked by the inhomogeneity of

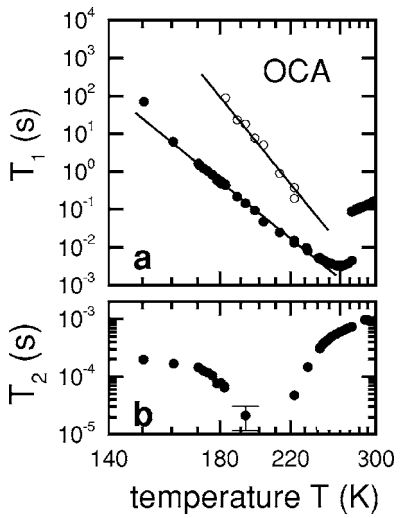


FIG. 3. (a) Spin-lattice-relaxation times $T_1$ of OCA. The closed symbols correspond to the measurements taken upon cooling and the open ones to those taken upon heating. The solid lines represent effective energy barriers of 5250 and 3450 K. Corresponding spin-lattice-relaxation times for MCA were published in Ref. 16. (b) Spin-spin relaxation-times of $T_2$ of OCA as measured using a solid-echo sequence.

the static magnetic field which was estimated from the absorption linewidth in the cubic phase to be about 1 kHz. The slow down of molecular motion leads to a decrease of $T_2$. Between 220 and 190 K, $T_2$ was so short that its accurate evaluation was not possible. Extremely short $T_2$ values are indicative of molecular tumbling rates of the order of the deuteron linewidth of the rigid lattice which typically is on the order of $1/(1\ \mu s)$. Below the minimum the increase of $T_2$, expected when the molecular motion slows down further, is cut short by the transversal dipolar dephasing. At the lowest temperatures studied here we find $T_2 \approx 200\ \mu s$. The overall temperature dependence of MCA is quite similar to that of OCA (not shown). However, the temperature range in which $T_2$ is smaller than about 10 $\mu s$ is somewhat broader for MCA. This can be interpreted to signal a narrower width of the distribution of relaxation times as compared to OCA. Conversely for extremely broad distributions of relaxation times $T_2$ stays long enough so that measurements can reliably be taken.[26]

The slow down of molecular motion is also clearly recognized from $T_1$, see Fig. 3(a). Similar to the observations for MCA (Ref. 16) a $T_1$ minimum shows up near $T=260$ K just below the tetragonal to orthorhombic transition. It indicates that the molecular correlation time is about $\tau_c = 0.62/\omega_L \approx 2.5$ ns. Upon further cooling the spin-lattice relaxation of OCA exhibits a thermally activated behavior. In one run the sample was equilibrated at 150 K and subsequently slowly heated with 6.5 K/day. The measurements recorded subsequently generally exhibited a bimodal saturation recovery, i.e., in addition to the $T_1$ values found during cooling a much slower contribution to the longitudinal magnetization recovery showed up. Since these experiments were all conducted in the slow-motion regime, the considerably longer relaxation times $T_1$ imply a much slower molecular dynamics. We associate this behavior with the "sluggish" transition to phase IV reported[27] to occur near 167 K. However, we found evidence for such an order↔disorder transition already at $T \approx 172$ K. In Fig. 2 we show the magnetization trace of a sample which was rapidly cooled to this temperature and then aged for about 15 days. Within the experimental uncertainty the fast relaxing component reproduces the $T_1$ measured upon cooling. The other contribution was found to be about 176 times slower at this temperature. It accounts for about half of the total magnetization in this run. This ratio stabilized within about 5 days after reaching 172 K and then exhibited only a minor drift upon further annealing.

It is important to observe from Fig. 3(a) that the effective energy barrier deduced from the spin-lattice-relaxation times of phase IV via $\ln(T_1) \sim \text{const} + E/T$, amounts to $E=5250$ K. It is thus about 1.5 times larger than that of phase III (cf. the solid lines in this figure). Obviously the presumably ordered molecular packing in phase IV hampers the molecular reorientations quite effectively.

A quantitative analysis of these data in terms of the spectral densities $J(\omega)$ and of the fluctuating part $K_{Q,\text{eff}}$ of the electric-field gradient (EFG) tensor at the deuteron site will not be attempted. An analysis of $1/T_1 = K^2_{Q,\text{eff}}[J(\omega_L) + 4J(2\omega_L)]$ for MCA revealed that a simple, unique description could not be found for the orthorhombic phase.[16] The minimal $T_1$ of OCA is slightly longer than that of MCA. Since the quadrupolar coupling constants for the deuterons of both substances are practically identical, this implies that the distribution of relaxation times is somewhat narrower for MCA in harmony with what above was concluded on the basis of the $T_2$ measurements.

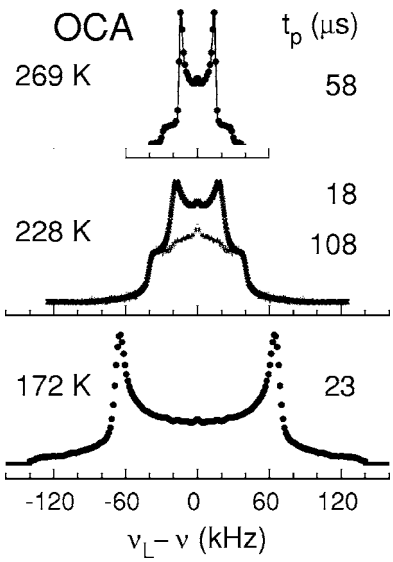


FIG. 4. Deuteron solid-echo spectra of OCA for various temperatures are represented by symbols. For $T=269$ K the solid line reflects a Pake-type shape with $\delta = 2\pi \times 29.4$ kHz. For $T=228$ K two spectra are presented which differ for smaller frequencies but agree for larger ones. The dependence on the pulse spacing $t_p$ here is different from what would be expected for the reorientational motions dominated by small-angle jumps. A spectrum in the rigid-lattice regime ($T=172$ K) is also shown.

### B. NMR spectra

A different perspective on the molecular dynamics is offered by the acquisition and analysis of absorption spectra. We recorded deuteron solid-echo spectra for OCA and MCA. In the tetragonal and the cubic high-temperature phases narrow liquidlike lines were obtained, indicative for a quasi-isotropic molecular motion, while at low temperatures we found Pake-type patterns, Fig. 4. The rigid-lattice (RL) spectrum recorded for OCA at 172 K corresponds to a quadrupolar anisotropy parameter $\delta_{\text{RL}}/2\pi = \frac{3}{4}e^2qQ/h = 135.9$ kHz and a vanishingly small anisotropy parameter. At this temperature the motional correlation time $\tau_c$ is thus much longer than $1/\delta = 1.2\ \mu s$. When $\tau_c$ is of the same order as $1/\delta$ the NMR line shape becomes heavily distorted. As an example in Fig. 4 we show the solid-echo spectra recorded at 228 K for pulse spacings of 18 and 108 $\mu s$. It is seen that for a large spacing the edge singularities of these spectra practically vanish. This contrasts with the observations for supercooled liquids.[28] There, due to the presence of relatively small jump angles (close to the glass transition typically 10°), an increase of the pulse spacing leads to a sharpening of the singularities. At higher temperatures, the spectra for OCA exhibit a motionally narrowed Pake-type shape, which reveals that the molecular motion in this crystal is highly anisotropic.

During the course of the present work we studied the

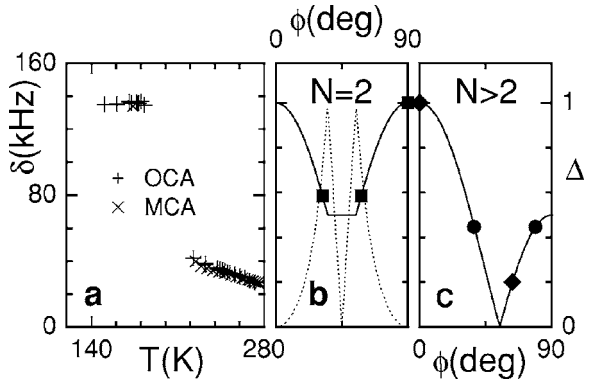


FIG. 5. The temperature dependence of the effective quadrupolar coupling of the solid-echo spectra of the carboranes is shown in frame (a). The scale on the right-hand side gives the coupling constants normalized by their low-temperature ($T<190$ K) value $\delta_{RL}/2\pi=135.9$ kHz, i.e., $\Delta=\delta(T)/\delta_{RL}$. The solid lines in frames (b) and (c) show the reductions of the spectral width as expected for cone models with $N=2$ and $N>2$ equivalent sites, respectively. The half opening angle on which the CD bonds move during the reorientation process are denoted by $\phi$. For $N=2$ the asymmetry parameter $\eta$ is represented by the dashed line, for $N>2$ this parameter vanishes. The normalized couplings associated with a motion about the various symmetry axes of the ideal icosahedron are represented by squares ($C_2$ axis), circles ($C_3$ axis), or diamonds ($C_5$ axis).

partially narrowed spectra in a systematic fashion. The anisotropy parameters $\delta(T)$ estimated from the splitting of these spectra are collected in Fig. 5. The rigid-lattice linewidth of MCA is compatible with that of OCA. It is seen that for both substances $\delta$ as normalized to its low-temperature value, i.e., the reduction factor $\Delta\equiv\delta/\delta_{\mathrm{RL}}$, increases from about 0.2 near the tetragonal to orthorhombic phase transition to about 0.3 near 220 K. For somewhat lower temperatures NMR spectra could not be measured reliably since spin-spin relaxation became very fast, cf. Fig. 3(b). At $T<190$ K, when $T_2$ turns longer again, the anisotropy parameter is maximum and practically temperature independent for both substances.

Partially averaged spectra typically indicate the existence of rapid anisotropic molecular motions about some symmetry axis.[29] In the carboranes the CD bonds can enclose various angles with the pseudo-$C_2$, pseudo-$C_3$, and pseudo-$C_5$ molecular axes. For motions about the latter two axes the reduction factors are simply given by the second Legendre polynomial[30]

$$\Delta(\phi)=\tfrac{1}{2}(3\cos^2\phi-1), \tag{1}$$

with $\phi$ denoting half of the opening angle of the cone along which a CD bond moves. In Fig. 5(c) we graphically display the possible angles and the resulting reduction factors expected for $N$-fold jumps among $N\geqslant 3$ equally populated sites. Figure 5(b) represents the analogous plot for $N=2$. As these figures show, none of these simple rotational motions alone can explain the observed behavior. However, if one assumes the existence of a composite molecular motion[17] it is possible to rationalize the continuous temperature variation of $\Delta$. We will come back to this point in Sec. V below.

In the rigid-lattice regime no dynamical and geometrical information can be retrieved from one-dimensional spectra other than that the rates characterizing the molecular motions

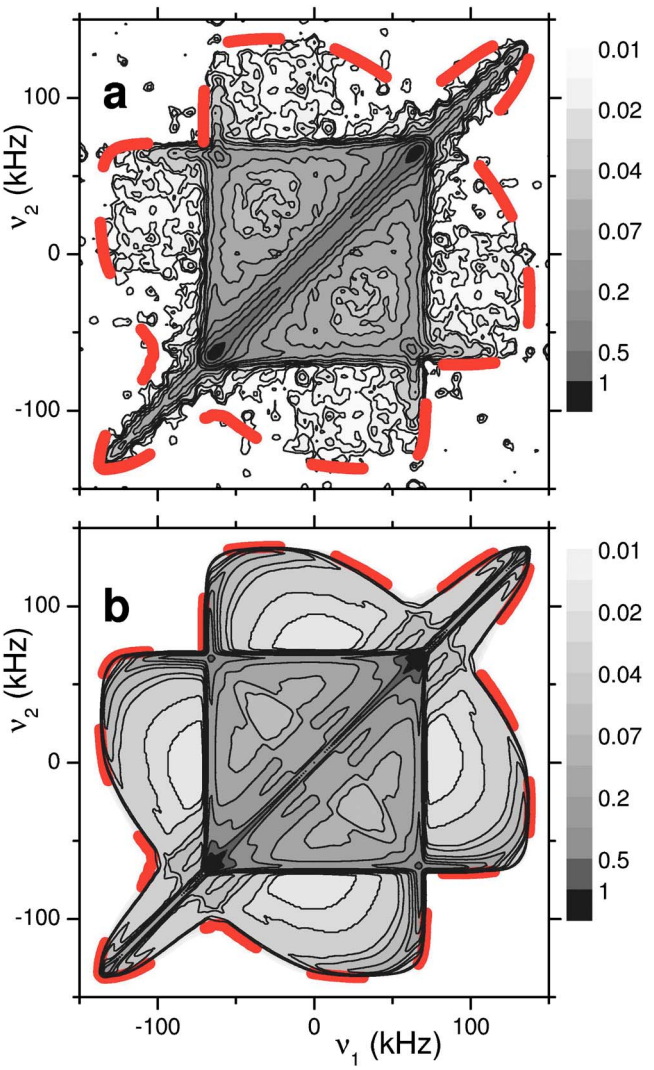


FIG. 6. (a) Contour plot of the 2D exchange spectrum measured for OCA at $T=172$ K. The grey scales represent the relative spectral intensity. (b) Contour plot of the simulated spectrum corresponding to the tilt-jump model. The exchange intensity comprises a number of elliptical ridges stemming from different jump angles, but is dominated by one which corresponds to the icosahedronlike jump motion as defined in Sec. IV. The associated angle of $\theta_5=2\arctan\sqrt{(3+\sqrt{5})/(7+3\sqrt{5})}\approx 63.43°$ is marked by thick broken lines in both frames.

are smaller than $\delta_{\mathrm{RL}}$. Therefore at lower temperatures we recorded two-dimensional (2D) exchange spectra using a five-pulse technique[31] with the solid-echo delays between the first and second as well as between the fourth and fifth pulses set to 30 $\mu$s. The length of the $\pi$ pulse here was 5.6 $\mu$s and the recycle delay was 7 s. The 64 traces with an increment of 2 $\mu$s were recorded in the indirect ($t_1$) domain. In the direct ($t_2$) dimension 1024 data points were collected with sampling intervals of 1 $\mu$s. Gaussian damping (with a variance of 100 $\mu$s), zero filling, and symmetrization were applied in both dimensions. The sin-sin and cos-cos spectra were recorded separately and added with appropriate weighting.

A 2D spectrum of OCA thus obtained at $T=172$ K for a mixing time of $t_m=1$ ms, which roughly corresponds to the average correlation time, is shown in Fig. 6(a) as a contour plot. The off-diagonal intensity is smeared over large ranges of the spectral plane, indicating that large reorientation

angles $\beta$ are involved in the motional process. Elliptical ridges, with an aspect ratio of the small to the large semiaxis $b/a=\tan\beta$, are expected in this representation if a well-defined angle $\beta$ is present.[29] However, it is obvious from the experimental data that a clear-cut ridge pattern was not detected. Rather, there seems to be a distribution of reorientation angles governing the molecular dynamics of OCA. In order to obtain an estimate of the largest angle within this distribution we included the elliptical patterns into Fig. 6(a) that correspond to an angle of $\beta=63°$. This is the reorientation angle of a CD bond expected for a nearest-neighbor jump which we define such that it moves the position of a vertex of the molecular icosahedron onto an adjacent vertex. The fact that most of the spectral intensity seen in Fig. 6(a) is localized near the diagonal part of the spectrum suggests that a significant fraction of the reorientation events also involves small angles. Alternatively one may speculate that the large-angle motions are slow while the small-angle motions are fast on the scale of $t_m$.

### C. Two-time correlation functions

The reorientation of the carborane molecules can be monitored quite directly using the two-time stimulated-echo technique which yields $F_2^X(t_p,t_m)\propto\langle X[\omega_Q(0)t_p]X[\omega_Q(t_m)t_p]\rangle$ with $X$ being the sine or the cosine of the phase angle $\omega_Q t_p$. Here the polar angle $\Theta$ of a CD bond with respect to the static external magnetic field is encoded by the quadrupole perturbed precession frequency $\omega_Q(t)=(\delta/2)[3\cos^2\Theta(t)-1]$. We have acquired $F_2^X(t_p,t_m)$ functions for a number of evolution times $t_p$ and for several temperatures. The measurements recorded for MCA at $T=172$ K as a function of $t_m$ are shown in Fig. 7(a) for $t_p=1$ $\mu$s and 60 $\mu$s. For $X=\sin$ and $t_p\rightarrow 0$, the decay yields the rotational correlation time $\tau_c$. It is seen that the correlation time is almost independent of $t_p$.

In Fig. 7(b) we present some temperature-dependent stimulated-echo functions for OCA which show the two-step decay of $F_2^X$. This behavior originates from the orientational decorrelation at shorter times and the decay of Zeeman order ($X=\cos$, given by $T_1$) or of spin-alignment order ($X=\sin$, given by $T_{1Q}$) at longer times. The data can thus be described using the expression

$$F_2^X(t_p,t)=\{A_1(t_p)+A_2(t_p)\times \times\exp[-(t/\tau_2(t_p))^{\beta(t_p)}]\}\exp(-t/T_{1(Q)}). \quad (2)$$

It implies an exponential longitudinal spin relaxation and a nonexponential loss of orientational correlation, parametrized by the Kohlrausch exponent $\beta$. The latter describes the stretching of the correlation and is typically between 0.5 and 0.6. The evolution time dependence of the time scales $\tau_2(t_p)$ is presented for OCA and MCA in Fig. 8 for $T\approx 172$ K and compared with the data on glycerol,[32] a typical supercooled liquid. It is seen that in the crystalline materials $\tau_2$ is essentially constant and only at very long $t_p$ the time constants exhibit a slight decrease. This shows that here the large-angle jumps play a dominant role, in contrast to the molecular reorientation of viscous liquids for which the mean jump angles are typically of the order of 10°.

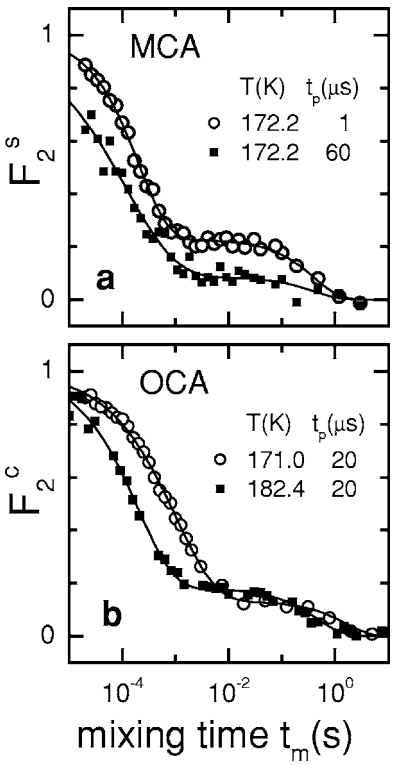


FIG. 7. (a) Two-time stimulated-echo functions $F_2^s(t)$ recorded for MCA at $T=172.2$ K for short and long evolution times $t_p$. (b) Two-time stimulated-echo functions $F_2^c(t)$ of OCA recorded for two different temperatures and $t_p=20$ $\mu$s. The lines in both frames are fits using stretched exponential functions, Eq. (2).

Most of the detailed measurements that we will present in the following were conducted at a temperature of 172 K for the following reason: For much lower temperatures the spin-lattice-relaxation times become longer which would result in excessive data accumulation periods. For much higher temperatures the correlation times move closer to the lower threshold of the experimental time window. This would hamper an accurate determination of the parameters affecting the shape of the $F_2$ functions and their limiting values, $A_1$ and

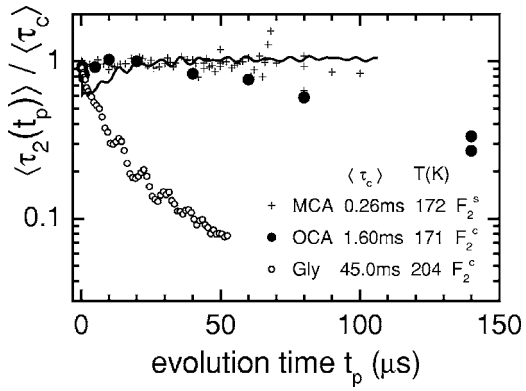


FIG. 8. Decay constants $\tau_2(t_p)$ characterizing the two-time correlation function for a range of evolution times. To compare the patterns from the plastic crystals OCA and MCA with that from the supercooled liquid glycerol (Gly), the data have been normalized to the correlation time $\tau_2(t_p\rightarrow 0)$. It is clearly seen that the pronounced decay of the pattern seen for glycerol, stemming from the dominant fraction of small (2°–3°) angles in its jump angle distribution, is absent for the carboranes.

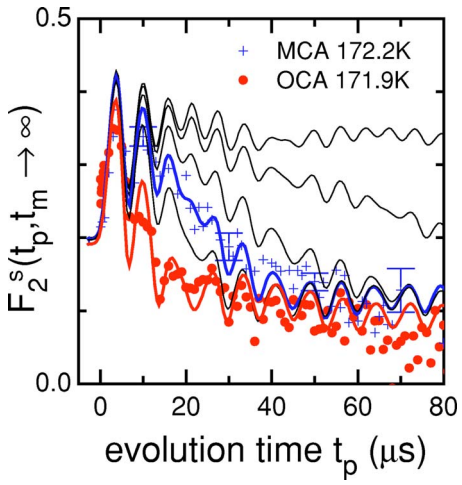


FIG. 9. The symbols represent the evolution time dependence of the final state amplitudes of OCA and MCA. The lines correspond to results of computations using the tilt-jump model to be discussed in Sec. IV, below. The adjustable parameter here is the tilt angle. If it is chosen as $\theta_t=0°$, corresponding to simple 120° jumps, it leads to the line oscillating near 1/3. For larger angles of 1°, 2°, 3°, 4°, and 7° the final state amplitude of 1/12 is approached successively more quickly.

$A_2$. However, an accurate knowledge of these coefficients is required since from them the final plateau value $Z^X(t_p)=A_1(t_p)/[A_1(t_p)+A_2(t_p)]$ characterizing the reorientational geometry can be evaluated.

In Fig. 9 we present the final plateau values $Z^{\sin}(t_p)$ for OCA (see also Ref. 17) and for MCA. Already the limiting behaviors of these patterns are quite instructive. For large $t_p$ the plateau value approaches $Z \to 1/(12\pm2)$ which via $N=1/Z$ reflects the number of magnetically inequivalent positions. It should be noted that for simple rotational motions about the $C_2$, $C_3$, or $C_5$ (pseudo) axes one expects at most six resonance lines, due to the inversion symmetry characterizing the ideal icosahedron. Another remarkable feature is that for relatively small but finite evolution times plateau values compatible with $Z=1/3$ are seen indicative for a motion involving three sites. Since for small $t_p$ the angular sensitivity of the $F_2$ function is relatively poor, this is taken as a hint that this motion is one about a threefold axis involving quite large angles. In order to rationalize $N \approx 12$ in the limit $t_p \to \infty$ one may thus assume that each $C_3$ axis can point along four directions. Finally, for $t_p \to 0$ it is seen that $Z$ is close to 0.2. For simple cone motions from $Z(0)$ one may infer the half opening angle $\phi$ of the cone. If more than two sites are involved and if they are all equally populated then[33] $Z^{\sin}(0)=3/2(\cos^4\phi+1/2\sin^4\phi)-1/2$. It turns out that, e.g., the $C_3$ as well as the $C_5$ motion give $Z=0.2$ if the contributions associated with the angles obvious from Fig. 5(c) are properly weighted.[34]

### D. Four-time correlation functions

Even more detailed insight into the orientational relaxation dynamics of the carboranes can be gained from the measurement of four-time stimulated-echo functions of the type $E_4^{XY}(t_{m1},t_{m2},t_{m3}) \propto \langle X(\omega_1 t_p)X(\omega_2 t_p)Y(\omega_3 t_p)Y(\omega_4 t_p)\rangle$. Here $X(\omega_k t_p)$ stands for either $\cos(\omega_k t_p)$ or $\sin(\omega_k t_p)$ and the same holds for $Y(\omega_k t_p)$. The index $k$ numbers the four evolution periods which bracket the three mixing times $t_{mi}$. In practice one varies but a few of the time intervals determining this multidimensional $E_4$ function.[35] In the present and in our previous[17] experiments we keep $t_p$ fixed in a given run. A sequence of seven properly phased radio-frequency pulses is usually employed to generate the various sine, cosine, and mixed variants of $E_4^{XY}(t_{m1},t_{m2},t_{m3})$ which are then co-added with appropriate weighting.[36]

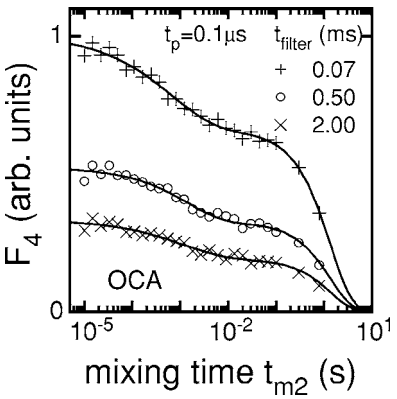


FIG. 10. Four-time correlation function $F_4$ as measured for OCA at $T=170.4$ K for different mixing times $t_{m1}=t_{m3}$. The nominal evolution time, i.e., the shortest time between the pulses was 0.1 μs. The fits were done with stretched exponential functions including a term accounting for spin-lattice relaxation. The latter takes place on a time scale of $T_1=1.4$ s.

Even for a fixed $t_p$ a number of different experiments is still possible. We carried out the following ones: (i) The function which is obtained by fixing $t_{m1}=t_{m3}$ and varying the central mixing time is usually termed $F_4$ if $t_p\delta \gg 1$. It has been used previously to monitor dynamical exchange processes.[29,35] (ii) In the operational limit $t_p \to 0$ the same function has sometimes been named $L_4$.[37] It has been shown for an isotropic reorientation process that in the absence of dynamical exchange, $L_4$ should not decay to below 7/15 before longitudinal relaxation sets in. As we have pointed out earlier,[25] the limit $t_p \to 0$ is hard to reach in practice. Therefore the experiments carried out for relatively small evolution times will nevertheless also be designated $F_4$. (iii) Alternatively, if one fixes $t_{m1}$ and $t_{m2}$ (usually the latter is chosen rather short) and varies $t_{m3}$ one obtains the function $G_4$. In each case these experiments are quite time consuming due to the often significant loss of magnetization occurring during each evolution and mixing time. The loss of signal due to spin-lattice and/or spin-spin relaxation is not included in the above expression for $E_4$.

For the current work we measured the four-time correlation functions of only one of the substances; we have chosen OCA. Some results were already published elsewhere[17,25] and particularly the decay of $G_4$ and $F_4$ as measured for relatively long $t_p$ has been discussed. In Fig. 10 we present the raw data for $F_4(t_{m2})$ for various $t_{m1}=t_{m3}=t_{filter}$ and $t_p=0.1$ μs. These functions exhibit a decay on the microsecond scale and another one at longer times due to spin-lattice relaxation. When corrected for the latter the curves do not decay to below 7/15 of their initial value. It must be remembered that this number corresponds to that expected for isotropic motion. Before we argued that the molecular motion in the carboranes is not isotropic. Therefore the significance of

the findings implied by Fig. 10 can be discussed only on the basis of a given model characterizing the anisotropic motion.

## IV. STOCHASTIC JUMP MODELS

In order to describe the reorientational motion of OCA on the time scale of microseconds and longer, we consider stochastic jump models. We thus assume that the molecules reside in a particular orientation until a sudden jump around a preferred axis occurs. We consider Markovian jump processes which enables a detailed calculation of all relevant quantities. In this case all probabilities can be obtained uniquely from the conditional probability $P_{kl}(t,t_0)$ of finding a molecular orientation $\Omega_k$ at time $t$ given an orientation $\Omega_l$ at an earlier time $t_0$. We furthermore restrict ourselves to stationary processes which means that $P_{kl}(t,t_0)$ only depends on the time difference, $P_{kl}(t,t_0)=P_{kl}(t-t_0)$. This conditional probability (or Green's function) obeys a master equation,[38]

$$\frac{\partial}{\partial t}P_{kl}(t)=\sum_{m=1}^{N}\Pi_{km}P_{ml}(t). \tag{3}$$

Here, the $\Pi_{km}$ are the elements of the matrix of transition rates and $N$ is the overall number of orientations considered. In the present context we are interested in the two-time and four-time correlation functions introduced in the preceding sections. As an example, $E_2^X(t_p,t_m)$ can be calculated according to

$$\begin{aligned}E_2^X(t_p,t_m)&=\langle X[\omega_Q(0)t_p]X[\omega_Q(t_m)t_p]\rangle\\&=\sum_{k,l=1}^{N}I_{kl}^X(t_p)P_{kl}(t_m)W_l,\end{aligned} \tag{4}$$

where $W_l$ denotes the equilibrium population of orientation $\Omega_l$. Because we are dealing with powder samples all orientations occur with equal probability and the ensemble average $\langle\cdot\rangle$ includes the powder average

$$I_{kl}^X(t_p)=\langle X[\omega_Q(\Omega_k)t_p]X[\omega_Q(\Omega_l)t_p]\rangle_{\text{powder}}. \tag{5}$$

In this expression $\omega_Q(\Omega_k)$ is a geometrical quantity that can be computed from the assumed geometry of a given jump model. These averages are performed numerically for arbitrary $t_p$, but limiting values for $t_p\to 0$ and $t_p\to\infty$ can be given analytically for $X=\sin,\cos$. Therefore, once the transition rates and the connectivity of the different orientations involved in a specific model are fixed, the relevant correlation functions can be calculated from the solution of the master equation (3). For the four-time correlation functions similar expressions can be given due to the Markovian nature of the processes considered.

Since the molecular shape is almost that of an ideal icosahedron, it is tempting to assume that reorientations take place around the icosahedral symmetry axes. It is well known that in such a case group-theoretical methods can be used to calculate arbitrary correlation functions.[39] Below we focus on the results of such a calculation and for details we refer to Ref. 34.

In the Experimental section it was found that 12 magnetically inequivalent sites are available for each deuteron. Let us first consider that the 12 sites are occupied with an equal probability of $W=1/12$. In the simplest case, all jump rates are the same, denoted by $r$. Then the matrix of the transition rates is given by $\Pi_{ik}=r(1-12\delta_{ik})$. The master equation (3) for this problem can be solved and one finds:

$$\begin{aligned}P(\Omega_k,t|\Omega_i)|_{i=k}&=P_{ii}=\tfrac{1}{12}+\tfrac{11}{12}e^{-t/\tau}=P^{(1)},\\P(\Omega_k,t|\Omega_i)|_{i\neq k}&=P_{ki}=\tfrac{1}{12}-\tfrac{1}{12}e^{-t/\tau}=P^{(2)},\end{aligned} \tag{6}$$

with $\tau=1/(12r)$. Since the two conditional probabilities are characterized by the same time constant, the two-time correlation function $F_2^X(t_m)$ decays in a single-exponential manner. Using Eqs. (4) and (5) the echo signal can be written as

$$\begin{aligned}E_2^X(t_m)&=\sum_{ki}I_{ki}^XP_{ki}(t_m)W_i\\&=\tfrac{1}{12}[P^{(1)}(12I_{11}^X)+P^{(2)}(12I_{11}^X+120I_{21}^X)].\end{aligned} \tag{7}$$

For $t_p\to\infty$ one finds $I_{11}^X=1/2$ and $I_{21}^X=0$ which means that $F_2^X$ decays to $1/6$ of its initial value. In other words, in the limit of large $t_p$, one finds the simple expression,

$$F_2^X(t_m)|_{t_p\to\infty}=E_2^X(t_m)/E_2^X(0)|_{t_p\to\infty}=\tfrac{1}{6}+\tfrac{5}{6}e^{-t/\tau}. \tag{8}$$

The most important point is that the residual correlation is given by $1/6$ instead of the experimentally observed value of about $1/12$. The reason for this factor of $1/6$ is simply that due to the inversion symmetry of an icosahedral molecule the deuterons are pairwise magnetically equivalent.

If instead of assuming a common rate $r$, one allows for different rates for reorientations around the various pseudo-two-, three-, and fivefold axes of the icosahedron, one again finds Eq. (7) for $E_2^X(t_m)$, with the only difference that $1/\tau$ now is given by a linear combination of the reorientation rates involved.[34]

The discrepancy between the prediction of the simple model considered here and the experimental findings rules out pure icosahedronlike jump motions as a useful model to describe the reorientational process of the carboranes. Here we define the icosahedronlike jump motions as one which only involves two-, three-, and fivefold rotations around the (pseudo-) $C_2$, $C_3$, and $C_5$ axes, respectively, or combinations thereof.

Thus in any case the question arises as to what kind of model can represent the reorientational behavior. The model has to involve 12 inequivalent orientations in order to correctly meet the experimental plateau values. Furthermore, this requirement provides only one constraint. A realistic description should of course fit all the experimental data with the same set of parameters. The most natural assumption when considering possible candidates is that reorientations around symmetry axes still play a dominant role. Similar to the situation in $C_{60}$ (Refs. 40–43) one could assume that the reorientations take place around the twofold symmetry axis and that there are different orientations of this axis in the crystal.

If one assumes that the molecule only reorients via the different pseudo $C_2$ axes this leads to six nonequivalent NMR frequencies. One then has to assume the two distinct orientations of the molecules in order to allow for 12 different frequencies. This model was calculated[34] and it turned

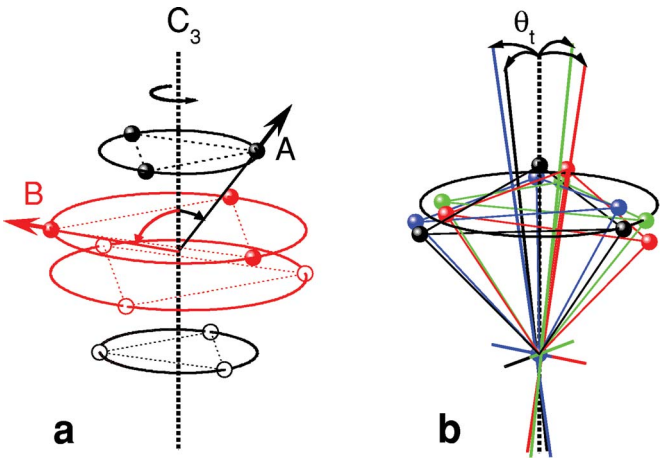


FIG. 11. (Color) (a) The dots represent the vertices of an icosahedron. To guide the eyes, deuterons lying in a common plane perpendicular to the molecular $C_3$ axis are connected to form regular triangles. Those with the larger distance from the rotation axis, i.e., the inner ones, are designated population $A$ and the outer ones population $B$. The arrows point radially outwards from the center of the icosahedron and are used to define the angles $\phi_B=37.4°$ (which is identical to $\theta_3$) and $\phi_A=\arctan\sqrt{14+6\sqrt{5}}=79.2°$. (b) The molecular $C_3$ axis is tilted about an angle $\theta_t$ with respect to the local, crystal-fixed symmetry axis, here represented by the dashed line. The four orientations of the icosahedral molecules, allowed within the present tilt-jump model, are represented by the decorated triangles.

out that $F_2^s(t_p<40\ \mu\text{s}, t_m\to\infty)$ is a factor of 2 too low. On the other hand, the temperature dependence of the one-dimensional NMR spectra is most easily interpreted in terms of a threefold motion, see Sec. III B. Also the final correlation for small $t_p$ of the two-time correlation functions hints towards a pseudothreefold motion, see Sec. III C.

In the following we assume that reorientational jumps occur around the threefold ($C_3$) axes of OCA. Now, in order to obtain 12 nonequivalent NMR frequencies four distinct $C_3$ axes are needed. This means that there are four molecular orientations between which a jump can take place. The model we consider can thus be characterized in the following way. We have four possible orientations of an icosahedron in the crystal, each one corresponding to a well-defined orientation of a $C_3$ axis in space. These axes are tilted with respect to a crystal-fixed axis by a certain tilt angle, which is one of the parameters of the model that will be formulated in the following. Let us denote the four $C_3$ axes by Greek letters and the three positions on each of the axes by Latin ones such that a given position is characterized, e.g., by $\alpha, i$. One further point that needs to be considered is the fact that there are two distinct angles between the corners of the icosahedron and the $C_3$ axes. These angles are indicated by the arrows in Fig. 11(a) and correspond to what we call population $A$ and population $B$, respectively. On average the probability for their occurrence may be expected to be the same. Therefore, unless specified otherwise we assume a ratio of $[A]/[B]=1$ for the possible deuteron species.

The geometry of the motional model, which we will denote as "tilt-jump model" is displayed in Fig. 11(b). Here the $C_3$ axes themselves are tilted away by an angle $\theta_t$ from a crystal-fixed axis (marked by the dashed line). In order to satisfy the constraint that 12 magnetically inequivalent positions should exist, the $C_3$ axes are required to point in four different directions. For simplicity, i.e., to keep the number of adjustable parameters small, these are assumed to be arranged in a symmetrical fashion, cf. Fig. 11(b).

The dynamics of this model are determined by the transition rates occurring in the master equation, which in the present context are written as $\Pi_{(\alpha,i|\beta,j)}, \alpha,\beta=1,2,3,4$ and the three orientations determined by the rotations about a given $C_3$ axis, $i,j=1,2,3$. Of course, there are many possibilities to choose these rates. In order to have as few parameters as possible, we assume that the threefold rotations take place with a constant rate $\Gamma_3$, which means $\Pi_{(\alpha,i|\alpha,j)}=\Gamma_3$ for $j\neq i$. For the tilt motion we assume a rate $R$ which is also constant and independent of the position of the initial and the final orientations of the $C_3$ axis involved, i.e., $\Pi_{(\alpha,i|\beta,j)}=R$ for $\beta\neq\alpha$ and arbitrary $i,j$. Thus, more formally, we have for the matrix element needed in the computation of the Green's function,[34]

$$\Pi_{(\alpha,i|\beta,j)}=\{\Gamma_3-(3\Gamma_3+9R)\delta_{i,j}\}\delta_{\alpha,\beta}+R(1-\delta_{\alpha,\beta}). \tag{9}$$

Here, the diagonal terms reflect the sum rule $\Pi_{(\alpha,i|\beta,i))}=-\Sigma_{\beta,j}\Pi_{(\beta,j|\alpha,i)}$. The matrix defined by the transition rates can be diagonalized with the eigenvalues $\lambda_0=0$, $\lambda_1=12R$ (threefold degenerate), and $\lambda_2=3\Gamma_3+9R$ (eightfold degenerate). The knowledge of these eigenvalues and the corresponding eigenvectors allow the calculation of the Green's function.[38] For the tilt-jump model we find the following closed expressions:

$$P_{(\alpha,i|\beta,i)}(t)=\tfrac{1}{3}G^{(0)}_{(\alpha,\beta)}(t)+\tfrac{2}{3}G^{(1)}_{(\alpha,\beta)}(t), \tag{10}$$

and

$$P_{(\alpha,i|\beta,j)}(t)=\tfrac{1}{3}G^{(0)}_{(\alpha,\beta)}(t)-\tfrac{1}{3}G^{(1)}_{(\alpha,\beta)}(t)\quad i\neq j. \tag{11}$$

Here, we have defined the functions

$$G^{(0)}_{(\alpha,\beta)}(t)=\tfrac{1}{4}+\left(\delta_{\alpha,\beta}-\tfrac{1}{4}\right)e^{-12Rt}, \tag{12}$$

and

$$G^{(1)}_{(\alpha,\beta)}(t)=\delta_{\alpha,\beta}e^{-(3\Gamma_3+9R)t}, \tag{13}$$

These functions, along with the determination of the tilt angle and the other geometrical parameters of the model as indicated in Fig. 11, are sufficient to calculate all the required correlation functions. As an example we give the expression for the two-time correlation function,

$$E_2^X(t_m)=D_0+D_1e^{-12Rt_m}+D_2e^{-(3\Gamma_3+9R)t_m}, \tag{14}$$

where the amplitudes $D_0$, $D_1$, and $D_2$ are the sums of powder averages of the form given by Eq. (5). The explicit evolution time dependence on the coefficients $D_i$ is given elsewhere.[34] When comparing Eq. (9) with Eq. (6) we see that now two distinct rates are relevant to describe, within the model, the dynamics of a single molecule. This means that the relaxation is nonexponential.

The four-time correlation functions defined by

$$X_4^{XY}(t_0,t_{m1},t_{m2},t_{m3};t_p) = \langle X(\omega(t_0)t_p)X(\omega(t_{m1})t_p)Y(\omega(t_{m2})t_p)Y(\omega(t_{m3})t_p)\rangle = \sum_{ijkl} I_{ijkl}^{XY} W_i(t_0)P(j,t_{m1}|i)P(k,t_{m2}|j)P(l,t_{m3}|k) \quad (15)$$

can be computed in a way similar to that just discussed. This in principle requires to calculate the $12^4$ integrals,

$$I_{ijkl}^{XY}(t_p) = \langle X[\omega_Q(\Omega_i)t_p]X[\omega_Q(\Omega_j)t_p]Y[\omega_Q(\Omega_k)t_p] \times Y[\omega_Q(\Omega_l)t_p]\rangle_{\text{powder}}. \quad (16)$$

For the model of jumps between icosahedral sites it turns out that due to the symmetry of the correlation function and to that of the reorientation process itself, the number of inequivalent integrals reduces to 14, cf. Ref. 34. This simplifies the computations considerably. The tilt-jump model requires the calculation of many more integrals.

Detailed calculations[34] show that already for the simple model leading to Eq. (7) a partial decay of the correlation function can occur as a function of $t_{m2}$, except for $t_{m1} \to 0$. Such a decay is remarkable since the simple model considered here is characterized by a single rate: For an intrinsically exponential process, no dynamic rate exchange is expected. Based on various theoretical treatments the decay of the correlation function $F_4$ is taken as evidence for the existence of a dynamical exchange process.[44–46]

It should be pointed out that the approaches just cited implicitly assume that the precession frequency is altered by each reorientation process and that the return probability is close to zero. These are reasonable assumptions when dealing with supercooled liquids and amorphous polymers. The model which leads to Eq. (7) is clearly incompatible with these presumptions since due to the inversion symmetry of the model it is evident that always two of the 12 sites are magnetically equivalent. Therefore one should be able to distinguish the two kinds of reorientation processes: one which *does* from one which does *not* lead to a change of the precession frequency $\omega_i$. Thus molecules jumping from site $i$ (with $\omega_i$) to site $j \neq i$ (with $\omega_j$) via a site characterized by $\omega_i$ appear slower than molecules jumping directly from $i$ to $j$. Processes of the latter type can thus lead to reorientations which are seemingly slower than implied by the rate $r$ assumed in the model.

## V. DISCUSSION

The tilt and jump model described in Sec. IV was used to compute the evolution time dependence of the final state amplitude $Z(t_p)$. The results for $F_2^{\text{sin}}$ as based on Eq. (14) are shown in Fig. 9 for various tilt angles $\theta_t$. If $\theta_t = 0$, then the molecular motion reduces to a threefold rotation. Hence we may expect that for sufficiently large evolution times $Z(t_p)$ is close to 1/3. This expectation is confirmed by the calculations, cf. Fig. 9. If $\theta_t > 0$, then in the limit of large evolution times $Z(t_p)$ approaches 1/12. In Fig. 9 we have chosen $\theta_t = 0°$, 1°, 2°, 3°, 4°, and 7° for the model calculations. They demonstrate that the limit of 1/12 is approached more rapidly if the tilt angle is larger. The comparison with the experimental data shows that the model is able to yield a quantitative description. The tilt angle that characterizes the molecular motion in OCA is significantly larger than that for MCA, despite the fact that practically the same temperature was studied for both substances. The resulting tilt angles of about 7° for OCA and about 3° for MCA are confirmed by analyzing not only the sin-sin but also the cos-cos data.[34]

Furthermore we checked the evolution time dependence of the decay constants of the two-time correlation functions on the basis of the tilt-jump model. Similar to the experimental data we find that the calculated time constants (see the solid lines in Fig. 8) show only very minor variations with $t_p$. Only the experimental decay times recorded for OCA at $t_p \geqslant 80$ $\mu$s are somewhat smaller than expected on the basis of our calculations.

The shape of the 2D spectrum of OCA is compatible with the prediction of the tilt-jump model. In the simulation of the 2D spectrum[34] [Fig. 6(b)] we also used a tilt angle of 7° and a good agreement with the experimental results is obtained. In particular, the blurring of the off-diagonal intensity and the shape of the circumference of the largest ridge is similar to what is observed in the experimental spectrum.

The tilt-jump model also provides a natural explanation for the gradual narrowing of the spectra as compiled in Fig. 5. For a composite rotation process around two axes the corresponding reduction factors, cf. Eq. (1), have to be multiplied. Thus the effective quadrupolar coupling constant is given by

$$\Delta = \delta(T)/\delta_{\text{RL}} = \Delta_t \cdot \Delta_3 = \tfrac{1}{2}(3\cos^2\theta_t(T) - 1)\tfrac{1}{2}(3\cos^2\theta_3 - 1). \quad (17)$$

Here $\theta_3 = \arctan\sqrt{8/(7+3\sqrt{5})} \approx 37°$ is the angle that each C–D bond encloses with a $C_3$ axis.[47] Using Eq. (17) one can thus derive the tilt angle from the data shown in Fig. 5. The results for OCA have been presented earlier[17] and for MCA they behave very similar as can be expected from Fig. 5(a). When extrapolated to low temperatures these data suggest that the tilt angle tends to vanish. In this case the motion of the molecule would be a simple one about a threefold axis. It may be speculated that in this limit a phase transition could occur upon cooling. Indeed, the tilt angles amount to only a few degree close to the transition into the ordered phases. Near to about 275 K at which the transition into the quasi-isotropic phases occurs upon heating, the tilt angles become rather large. Here the tilt angles are on the order of $\theta_3$ implying that the angular excursions are so large that essentially a "melting" of the crystalline anisotropy occurs.

Taken together it can be said that the tilt-jump model provides a good description of the two-time correlation functions and of the one-dimensional (1D) and 2D spectra. This suggests that the occurrence of the four tilt axes reflect the impact of the crystal field on the molecular motions. However, as additional model calculations show there is some flexibility in choosing the four tilt axes in a less symmetrical fashion than implied by Fig. 11(b) and still obtain reasonable agreement with the data shown in Fig. 9.

To gain a view on the temperature dependence of the dynamics, in Fig. 12 we compare the time constants as obtained for $\tau \geqslant 1$ $\mu$s from dielectric spectroscopy[3,22] with

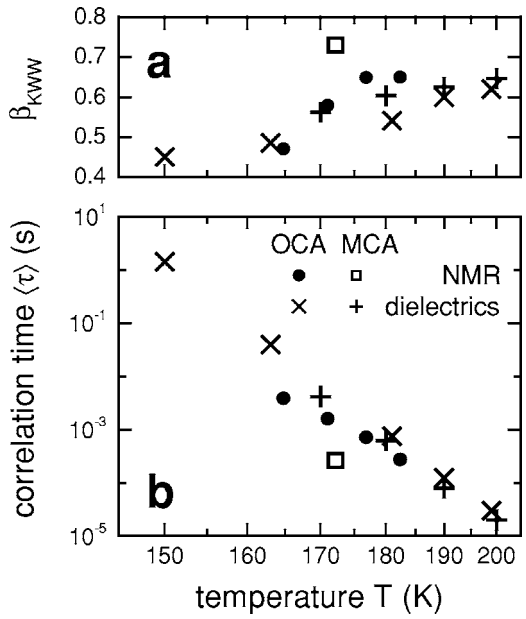


FIG. 12. Comparison of (a) stretching exponents and (b) time constants for OCA and MCA taken from dielectric spectroscopy (Refs. 3 and 22) and from measurements of the decay of the stimulated-echo functions recorded for $t_p=25$ $\mu$s (this work).

those from the NMR results of the present study. Overall there is a good agreement of the correlation times deduced from both methods, in particular, for OCA. At low temperatures at which the correlation functions could be extracted from the stimulated-echo experiments it is also possible to compare their Kohlrausch exponents $\beta_{\mathrm{NMR}}$ with that deduced from dielectric measurements $\beta_\epsilon$. Again, within experimental uncertainty the stretching parameters from the two methods agree. It should be noted that for supercooled liquids it was systematically found that $\beta_{\mathrm{NMR}}<\beta_\epsilon$. In that case the results could be understood using a model in which dynamic heterogeneity was implemented using a free-energy model.[48]

Due to their special reorientation geometry the carboranes also provide new insights in connection with the studies of dynamic heterogeneities of disordered systems.[49] When trying to achieve low-pass filtering using the $G_4$ function we found that the time constants $\tau_4$ characterizing the selected subensembles showed relatively small variations with the filter time $t_{m1}$ (see Ref. 17). The latter is connected with the filter efficiency. In the previous dynamic low-pass filtering applications we defined the filter efficiency as FE $=1-F_2(t_{m2})$. Here $F_2(t_m)$ is a function which is normalized to unity for $t_m\rightarrow 0$ and essentially decays to zero for increasing mixing times on a time scale $\tau_2$. As we have seen (cf. Fig. 7) in our case a significant plateau value shows up. Therefore, we introduced the effective filter efficiencies, "FE" $\equiv 1-[F_2(t_{\mathrm{filter}})-Z(t_p)]/[1-Z(t_p)]$.[17] This definition ascertains that the theoretical ratio $\tau_4/\tau_2$ which previously was used to identify intrinsically exponential processes[50] is independent of the plateau value. For intrinsically exponential processes the ratio $\tau_4/\tau_2$ is expected to show a strong variation with FE. Its absence could be interpreted as an indication of an intrinsically nonexponential process.[17] In the carboranes it arises since there are obviously two-time scales, those governing the threefold jumps and those determining the fourfold tilt motions. As always in disordered systems these time scales are distributed. In order to describe the data quantitatively the mean tilt time had to be chosen somewhat larger than the mean time characterizing the threefold jumps.[17,34]

Hence one is tempted to suspect that there is the possibility of dynamic rate exchange which is intramolecular in nature. Such a process should then lead to a decay of the four-time correlation function $F_4(t_{m2})$ as has already been pointed out in Sec. IV, for the icosahedral type of motions. For the tilt-jump model we estimated that the intramolecular contribution can only rationalize the observed decay of $F_4$ (Refs. 17 and 34) for very long filter times. Thus, like various supercooled liquids,[35] also OCA exhibits evidence for a short-lived dynamic heterogeneity. In a dimethylsulfone crystal with frozen-in disorder, on the other hand, $F_4$ did not decay, as expected.[17]

So far we discussed the four-time stimulated echoes for finite evolution times. Previously, it has been argued that in the limit of $t_p\rightarrow 0$ and in the absence of dynamic exchange, the function $L_4\propto\langle\omega_1\omega_2\omega_3\omega_4\rangle$ should not decay to below 7/15 of its initial value. However, we recall that this statement holds only for the overall isotropic reorientation processes. We calculated the evolution time dependence of the plateau values of the four-time correlation functions for a number of filter times $t_{m1}=t_{m3}$ and a range of small $t_p$.[25] The results indicate that for the anisotropic tilt-jump model the isotropic limit of 7/15 is not observed for $t_p\rightarrow 0$. To complicate the situation further, it has to be pointed out that in the experiment the evolution time cannot be made infinitely short. This is because there is also quadrupolar evolution during the finite length of the radio-frequency pulses. Further discussions of this function[25] including a proposal on how to approach better the limit $t_p\rightarrow 0$ in the experiment can be found elsewhere.[51]

## VI. SUMMARY AND CONCLUSION

In this article we reported on a detailed study of the molecular crystals *ortho*- and *meta*-carborane using deuteron NMR. From measurements of the spin-lattice-relaxation times of OCA several phase transitions were clearly revealed thus complementing our previous experiments on MCA. We found that the orientationally ordered low-temperature phase exhibit a significantly longer spin-lattice-relaxation time and a higher activation energy than the disordered one. The magnitude of the quadrupolar coupling constants in the rigid-lattice regime is quite typical. However, a peculiar behavior is noted from the one-dimensional spectra at higher temperature. When the rotational time scales are of the order of $1/\delta$, the edge singularities of the Pake type tend to vanish with increasing pulse spacing. This behavior is to be contrasted with that for supercooled liquids for which, under similar conditions, the singularities become more pronounced. In the latter substances the behavior can be ascribed to the occurrence of the small jump angles governing the molecular dynamics of these materials.[28] At higher temperatures partially averaged symmetric ($\eta=0$) spectra are observed for OCA

and MCA which show a smooth temperature variation of the coupling constant. This behavior could be rationalized by the existence of a composite rotation process with at least one of the angles characterizing the jump process being temperature dependent. The most detailed insights into the geometry of reorientation were obtained by carefully recording two-time stimulated-echo functions for a wide range of mixing and evolution times in connection with a thorough theoretical analysis. The theoretical modeling was based on Markovian stochastic models that were formulated in terms of a simple master equation. Among the various models we have considered[34] in the present article we discussed the model of icosahedrallike jumps for its simplicity and the tilt-jump model because the latter is able to describe in detail our experimental data. While the first model is associated with only six magnetically nonequivalent molecular orientations, the latter gives rise to 12 such orientations. This is because the tilt-jump model involves a sequence of four small-angle tilts about locally preferred axes in conjunction with symmetry adapted threefold jumps. Best agreement with the experimental data was achieved when the jump rates for these two types of motion were distributed with slightly different mean. The tilt angles from the stimulated-echo data and the ones extrapolated from the one-dimensional spectra were in harmony with one another. Furthermore the shape of the exchange pattern recorded for OCA using a two-dimensional spectrum was found compatible with that expected on the basis of the tilt-jump motion.

Also the analysis of the four-time correlation functions was based on this motional model. Due to the finite return probability, which is determined by the inverse number of distinguishable molecular orientations, the simple notion of dynamic filtering breaks down in the limit of seemingly larger filter efficiencies "FE." Under these circumstances, the time constants of filtered and unfiltered subensembles tend to approach one another as confirmed by explicit computations (see also Fig. 3 of Ref. 17). The relatively weak variation of time constants measured in that article using various filtering conditions could be identified as an intermolecular nonexponentiality which, however, is not as pronounced as that of the macroscopic response. Another new finding that emerged on the basis of the stochastic models treated in the current article is that the correlation function $F_4$ for finite evolution times can exhibit a decay due to *intramolecular* exchange processes. However, such effects can only account for a minor fraction of the experimentally observed decay. This implies the existence of short-lived dynamic heterogeneity similar to what has been reported in NMR studies of supercooled liquids.

## ACKNOWLEDGMENTS

We thank Peter Lunkenheimer for supplying the dielectric data used in Fig. 12. The authors dedicate this article to Professor Dr. Alois Loidl on the occasion of his 60th birthday.

[1] P. Lunkenheimer, U. Schneider, R. Brand, and A. Loidl, Contemp. Phys. **41**, 15 (2000), and references cited therein.
[2] Relaxation in Complex Systems IV, K. L. Ngai, E. Riande, and M. D. Ingram, published as J. Non-Cryst. Solids **307–310**, 1-1080 (2002).
[3] R. Brand, P. Lunkenheimer, and A. Loidl, J. Chem. Phys. **116**, 10386 (2002).
[4] K. Adachi, H. Suga, and S. Seki, Bull. Chem. Soc. Jpn. **41**, 1073 (1968).
[5] U. T. Höchli, K. Knorr, and A. Loidl, Adv. Phys. **39**, 485 (1990).
[6] K. Binder and J. D. Reger, Adv. Phys. **41**, 547 (1992).
[7] K. Binder and A. P. Young, Rev. Mod. Phys. **58**, 801 (1986).
[8] A. Loidl and R. Böhmer, in *Disorder Effects on Relaxational Processes*, edited by R. Richert and A. Blumen (Springer, Berlin, 1994), p. 695.
[9] T. Shimada, T. Matsuo, H. Suga, and F. Lüty, J. Chem. Phys. **85**, 3530 (1986).
[10] J. Wang and G. P. Johari, Phys. Rev. B **68**, 214201 (2003).
[11] F. Affouard, E. Cochin, R. Decressain, and M. Descamps, Europhys. Lett. **53**, 611 (2001).
[12] S. A. Lusceac, I. Roggatz, P. Medick, J. Gmeiner, and E. A. Rössler, J. Chem. Phys. **121**, 4770 (2004).
[13] E. C. Reynhardt and S. Froneman, Mol. Phys. **74**, 61 (1991).
[14] R. H. Baughman, J. Chem. Phys. **53**, 3781 (1970).
[15] P. Beckmann and A. Wendel, J. Chem. Phys. **73**, 3514 (1980).
[16] M. Winterlich, H. Zimmermann, and R. Böhmer, J. Non-Cryst. Solids **307–310**, 442 (2002).
[17] M. Winterlich, G. Diezemann, H. Zimmermann, and R. Böhmer, Phys. Rev. Lett. **91**, 235504 (2003).
[18] E. F. Westrum and S. Henriquez, Mol. Cryst. Liq. Cryst. **32**, 31 (1976).
[19] O. Yamamuro, M. Hayashi, T. Matsuo, and P. Lunkenheimer, J. Chem. Phys. **119**, 4775 (2003).
[20] S. S. Bukalov, L. A. Leites, A. L. Blumenfeld, and E. I. Fedin, J. Raman Spectrosc. **14**, 210 (1983).
[21] Z. Gamba and B. M. Powell, J. Chem. Phys. **105**, 2536 (1996).
[22] P. Lunkenheimer and A. Loidl, J. Chem. Phys. **104**, 4324 (1996).
[23] R. Brand, P. Lunkenheimer, U. Schneider, and A. Loidl, Phys. Rev. Lett. **82**, 1951 (1999).
[24] U. Schneider, R. Brand, P. Lunkenheimer, and A. Loidl, Eur. Phys. J. E **2**, 67 (2000); P. Lunkenheimer and A. Loidl, cond-mat/0210067 (unpublished).
[25] R. Böhmer, G. Diezemann, G. Hinze, K. R. Jeffrey, and M. Winterlich, in *Magnetic Resonance in Materials Science*, edited by G. Webb (in press).
[26] S. Fausti and G. Hinze (unpublished).
[27] L. A. Leites, Chem. Rev. (Washington, D.C.) **92**, 279 (1992).
[28] M. Vogel and E. A. Rössler, J. Phys. Chem. B **104**, 4285 (2000).
[29] K. Schmidt-Rohr and H. W. Spiess, *Multidimensional Solid State NMR and Polymers* (Academic, London, 1994).
[30] V. M. Litvinov, V. Macho, and H. W. Spiess, Acta Polym. **48**, 471 (1997).
[31] D. Schaefer, J. Leisen, and H. W. Spiess, J. Magn. Reson., Ser. A **115**, 60 (1995).
[32] R. Böhmer and G. Hinze, J. Chem. Phys. **109**, 241 (1998).
[33] F. Fujara, S. Wefing, and H. W. Spiess, J. Chem. Phys. **84**, 4579 (1986).
[34] M. Winterlich, Ph.D. thesis, Fachbereich Physik, Universität Dortmund, 2003; http://eldorado.uni-dortmund.de:8080/FB2/ls3/forschung/2003/Winterlich
[35] R. Böhmer, G. Diezemann, G. Hinze, and E. A. Rössler, Prog. Nucl. Magn. Reson. Spectrosc. **39**, 191 (2001).
[36] G. Hinze, R. Böhmer, G. Diezemann, and H. Sillescu, J. Magn. Reson. **131**, 218 (1998).
[37] G. Hinze, G. Diezemann, and H. Sillescu, Europhys. Lett. **44**, 565 (1998).
[38] N. G. van Kampen, *Stochastic Processes in Physics and Chemistry* (North-Holland, Amsterdam, 1992).
[39] P. Rigny, Physica (Amsterdam) **59**, 707 (1972).
[40] W. I. F. David, R. M. Ibberson, T. J. S. Dennis, J. P. Hare, and K. Prassides, Europhys. Lett. **18**, 219 (1992).
[41] F. Yan, Y. N. Wang, and J. S. Liu, Europhys. Lett. **48**, 662 (1999).
[42] W. Schranz, A. Fuith, P. Dolinar, H. Warhanek, M. Haluska, and H. Kuzmany, Phys. Rev. Lett. **71**, 1561 (1993).
[43] R. M. Lynden-Bell and K. H. Michel, Rev. Mod. Phys. **66**, 721 (1994).
[44] H. Sillescu, J. Chem. Phys. **104**, 4877 (1996).
[45] S. C. Kuebler, A. Heuer, and H. W. Spiess, Phys. Rev. E **56**, 741 (1997).

[46] G. Diezemann, J. Chem. Phys. **107**, 10112 (1997).
[47] If rotations would proceed about a $C_2$ axis the relevant angle would be $\theta_2 = \arctan \sqrt{(3+\sqrt{5})/(7+3\sqrt{5})} = \theta_5/2$.
[48] G. Diezemann, R. Böhmer, G. Hinze, and H. Sillescu, J. Non-Cryst. Solids **235–237**, 121 (1998).
[49] It should be pointed out that also crystalline ion conductors show a finite number of sites and thus precession frequencies. Multiple-time stimulated-echo experiments on a crystalline silver conductor were recently published. See M. Vogel, C. Brinkmann, H. Eckert, and A. Heuer, Phys. Rev. B **69**, 094302 (2004).
[50] R. Böhmer, R. V. Chamberlin, G. Diezemann *et al.*, J. Non-Cryst. Solids **235–237**, 1 (1998).
[51] R. Böhmer and F. Kremer, in *Broadband Dielectric Spectroscopy*, edited by F. Kremer and A. Schönhals (Springer, Berlin, 2002), pp. 625–684.